Progress In Electromagnetics Research C, Vol. 126, 77–90, 2022

Low Profile, Wideband, High Gain CDRA with Microstrip Feed for ISM and C Band Applications

Manshree Mishra, Anil Rajput, Pramod Kumar Gupta, and Biswajeet Mukherjee*

Abstract—Modern wireless communication systems require low profile, high gain, and wideband antennas. To meet these requirements a low profile Cylindrical Dielectric Resonator Antenna (CDRA) is proposed with wide bandwidth and high gain for ISM and C-Band applications. The CDRA is excited with a 50 ohm microstrip feed line with $HEM_{12\delta}$, $HEM_{21\delta}$, and $HEM_{13\delta}$ modes being observed at 5.6 GHz, 7.4 GHz, and 8.6 GHz resonant frequencies, respectively. The perturbation on the basic CDRA leads to the excitation of higher order modes and also decreases the effective permittivity of the CDRA by a factor of 13.4%, thereby reducing the antenna's Q factor, which helps to broaden the antenna's operating frequency range. The proposed structure offers wide impedance bandwidth of 69.4% from 4.8 GHz to 9.9 GHz. A peak gain of 8.9 dBi at 9.4 GHz and 95% radiation efficiency at 5.6 GHz are observed. Additionally, the proposed CDRA has a small footprint of $1.12\lambda_0 \times 1.12\lambda_0$ with a low profile of $0.16\lambda_0$ where λ_0 is the wavelength of the lower cut-off frequency. The proposed antenna is fabricated and measured, and a close agreement is found between the simulated and measured results.

1. INTRODUCTION

For ingestible and implantable body antennas, microstrip antennas are proposed in [1] and [2]. The researchers prefer microstrip patch antennas for a variety of reasons, including their low profile and potential for miniaturization. However, metallic patch antennas have low gain and high loss at high frequencies due to the presence of conducting materials. So to resolve this problem Dielectric Resonator Antenna (DRA) is used because it offers high gain and design flexibility.

Dielectric resonators (DR) act as efficient radiators under suitable exciting conditions. The various advantages of DRA are high radiation efficiency, high gain, low dielectric loss, ease of excitation, high power handling capability, and wideband operation. Depending on the resonator shape and feeding techniques for various applications, the DRA can excite various electromagnetic modes. For designing the conventional DRAs, basic structures like rectangular, hemispherical, and cylindrical DRAs are well investigated. Conical DRA, split-cylinder DRA, cylindrical-ring DRA, cross DRA, and perforated DRA have also been reported and analyzed [3]. Researchers are interested in the cylindrical geometry because it provides one degree of freedom. As opposed to the hemispherical DRA, which has no degree of freedom, this gives the designer more flexibility. A variety of methods have been used to improve CDRA's performance characteristics.

Low profile CDRAs are still in a niche state of research. In order to accomplish a low profile, stacking is used where the low permittivity dielectric layer is positioned beneath the high permittivity dielectric layer, as indicated in [4]. In [5], for obtaining a wide bandwidth with a low profile, a DRA with a lattice structure is used. Various methods have been proposed to improve the gain of a CDRA [6–10]. In [6], a circular periodic EBG substrate with a mushroom-like structure is used to provide a 3 dB gain

Received 14 September 2022, Accepted 27 October 2022, Scheduled 2 November 2022

* Corresponding author: Biswajeet Mukherjee (biswajeet.26@gmail.com).

The authors are with the Department of ECE, PDPM Indian Institute of Information Technology, Design & Manufacturing, Jabalpur, India.

enhancement. In [7], a DRA is loaded with a corrugated circular ring shaped single layer double sided meta superstrate to enhance the peak gain to 11.9 dBi. In [8], for enhancing the gain of the antenna in the boresight direction engraved grooves on the sidewalls of rectangular DRA are investigated. In [9], by the use of an FSS reflector the gain of an antenna is enhanced by 5–6 dBi. Higher order modes are also used for enhancing the gain and bandwidth of the antenna in [10]. Apart from the higher order modes, several methods are used for improving the bandwidth of the antenna like stacking two or more dielectric layers [11], the perturbation on DRAs as explained in [12], cavity backed disk, stacked DRAs, Coplanar DRAs, Embedded DRAs, Tetrahedral DRAs [3], and multilayer cylindrical DRA (MCDRA) structures [13]. Several feeding techniques like a coaxial probe, microstrip line, slot aperture, and conformal feed are used to obtain a wide impedance bandwidth. In [14], a cylindrical DRA is excited by a coaxial and aperture coupled feed for achieving wide bandwidth and broadside radiation pattern.

In this paper, a low-profile CDRA excited by a microstrip feed line is investigated for high gain and wideband application. The basic CDRA is perturbed, which results in a 13.4% reduction in the effective permittivity of the antenna. As a result, the antenna's Q factor is decreased, and the working range is extended. The perturbation on the basic CDRA is applied to the excitation of the $\mathrm{HEM}_{12\delta}$ mode, which is a higher order mode. $\mathrm{HEM}_{12\delta}$ mode has a lower quality factor as than other modes like $\mathrm{HEM}_{21\delta}$ and $\mathrm{TM}_{01\delta}$ [15]. Therefore, it acts as a good radiator. $\mathrm{HEM}_{12\delta}$, $\mathrm{HEM}_{21\delta}$, and $\mathrm{HEM}_{13\delta}$ modes are excited at 5.6 GHz, 7.4 GHz, and 8.6 GHz, respectively. Further, the effect of air perturbation on the CDRA and the effective permittivity of the material are also studied.

2. ANTENNA DESIGN AND ANALYSIS

The CDRA is designed on CST studio using transient domain solver. The CDRA is constructed using Rogers TMM 10 ($\varepsilon_r = 9.2$) having $\tan\delta = 0.0022$ dissipation factor. The radius of the DRA is 20 mm, and the height is 10 mm. It is loaded on the top of a feed line, and the feed line is etched on a Rogers RT5880 substrate ($\varepsilon_r = 2.2$) with a thickness of 1.57 mm. Figure 1 shows the design of the proposed CDRA. The width W_1 and length L_1 of the structure, on which the DRA is placed, are 70 mm and 70 mm, respectively. The DRA is excited by the microstrip feed. The various dimensions of the CDRA are mentioned in Figure 1(a). Figure 1(b) shows the perspective view of the structure.

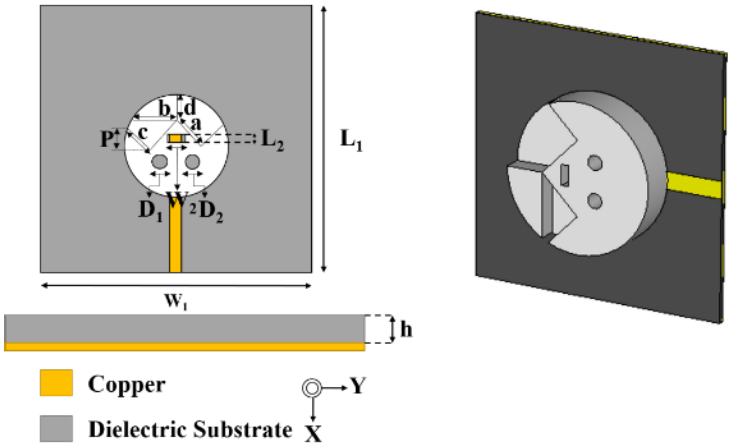

Figure 1. Cylindrical dielectric resonator antenna. (a) Dimensions from top view $R_1 = D_1/2 = 2$ mm, $R_2 = D_2/2 = 2$ mm, $L_5 = 2.5$ mm, $W_2 = 5.5$ mm, $L_3 = L_4 = 11.64$ mm, $L_2 = 10$ mm, $W_1 = 70$ mm, $L_1 = 70$ mm, $H = 1.57$ mm. (b) 3-D perspective view.

2.1. Antenna Design Methodology

The proposed antenna design process is depicted in Figure 2(a). Ant. 1 is designed to excite the fundamental $\mathrm{HE}_{11\delta}$ mode. The Vector H-field distribution of Ant. 1 verifies that $\mathrm{HE}_{11\delta}$ mode is excited

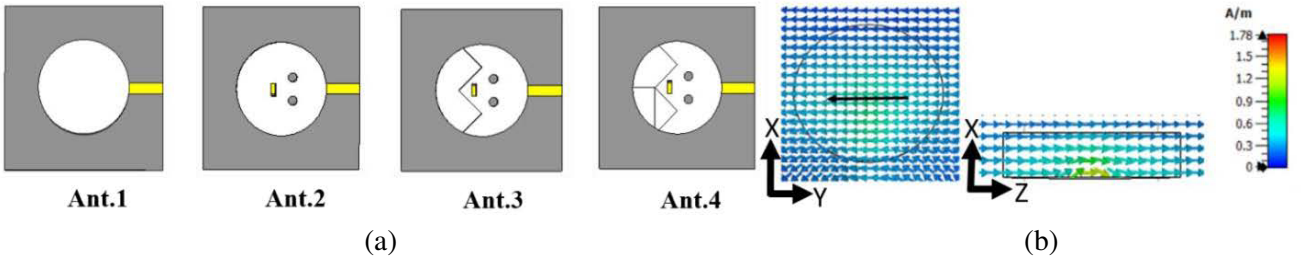

Figure 2. Various design topologies for the proposed structure. (a) Design methodology of the proposed cylindrical dielectric resonator antenna. (b) Vector H-field distribution of Ant. 1 along XY axis and XZ axis.

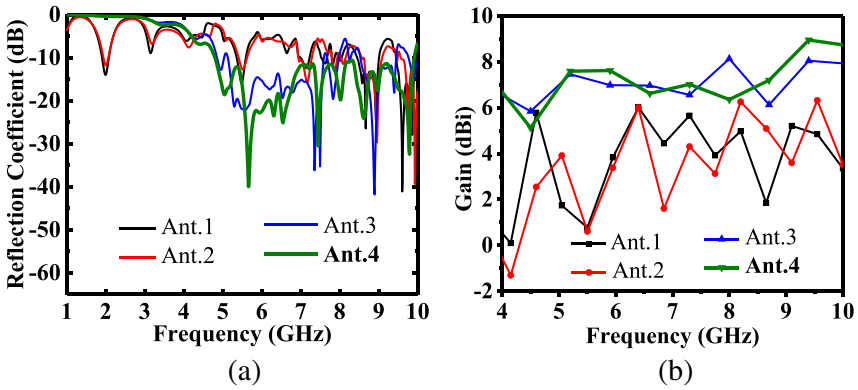

Figure 3. Comparison of all stages of the proposed design. (a) Reflection coefficient comparison of all the four steps antenna. (b) Gain comparison of all the four steps antenna.

as shown in Figure 2(b). The reflection coefficient comparison of all four steps of antenna is shown in Figure 3(a), and the gain comparison of all four steps of antenna is shown in Figure 3(b). The resonant frequency of Ant. 1 is calculated from Eq. (1) and Eq. (2) [3].

$$k_0 r = \frac{6.324}{\sqrt{\varepsilon_r + 2}} \left\{ 0.27 + 0.36 \frac{r}{2h} + 0.02 \left(\frac{r}{2h} \right)^2 \right\} \tag{1}$$

$$f_{\text{GHz}} = \frac{k_0 r \cdot 4.7713}{h_{\text{cm}} \cdot (r/h)} \tag{2}$$

where k_0 = free-space wave number, f_{GHz} = resonant frequency in GHz, r/h = aspect ratio of basic CDRA, r = radius of the cylinder in cm, h = height of the cylinder in cm, and ε_r = permittivity of the CDRA.

The calculated resonant frequency of the proposed design ($r/h = 2$, $r = 20\,\text{mm}$, $h = 10\,\text{mm}$, and $\varepsilon_r = 9.2$) is 2.9 GHz which can be verified from the reflection coefficient graph, shown in Figure 3(a). However, a small deviation is found between the calculated and simulated resonant frequencies because the equation becomes less accurate for extreme values of r/h (i.e., $r/h \ll 1$ or $r/h \gg 1$) [3].

The basic cylindrical dielectric resonator is altered by the perturbation of two cylindrical slots and one rectangular slot, i.e., (Ant. 2). Due to the perturbation effective permittivity is reduced which increases the resonant frequency and can be explained by the following equations [21].

$$\frac{\omega - \omega_0}{\omega} = -\frac{\iiint (\Delta\varepsilon E \cdot E_0^* + \Delta\mu H \cdot H_0^*)\, d\tau}{\iiint (\varepsilon E \cdot E_0^* + \mu H \cdot H_0^*)\, d\tau} \tag{3}$$

In the limit, as $\Delta\varepsilon \to 0$ and $\Delta\mu \to 0$, we can approximate E, H, ω by E_0, H_0, ω_0 and obtain

$$\frac{\omega - \omega_0}{\omega_0} \approx -\frac{\iiint \left(\Delta\varepsilon \left|E_0\right|^2 + \Delta\mu \left|H_0\right|^2\right) d\tau}{\iiint \left(\varepsilon \left|E_0\right|^2 + \mu \left|H_0\right|^2\right) d\tau} \tag{4}$$

E, H, and ω are the electric field strength, magnetic field strength, and resonant frequency of the perturbed cavity, respectively. E_0, H_0, and ω_0 are the electric field strength, magnetic field strength, and resonant frequency of the original cavity, respectively.

For Ant. 2 effective permittivity is 8.96 which is reduced by 2.6% resulting in an increased resonant frequency as shown in Figure 3(a). The calculation of effective permittivity is explained in Section 2.4. The parametric study is done on the two circular slots, and it is found that the effect of the first circular slot having radius R_1 and diameter D_1 affects both the bandwidth and gain. The bandwidth is increased towards the lower frequency as shown in Figure 4(a), and the gain also improves towards the lower frequency as shown in Figure 4(b). For $R_1 = 2\,\text{mm}$, wide impedance bandwidth of 29.12% is obtained which is greater than the other compared radius as shown in Figure 4(a). Impedance bandwidth is increased when the air is introduced into the perforated region which reduces the effective permittivity. Therefore for $R_2 = 2\,\text{mm}$ second circular slot having radius R_2 and diameter D_2 improves

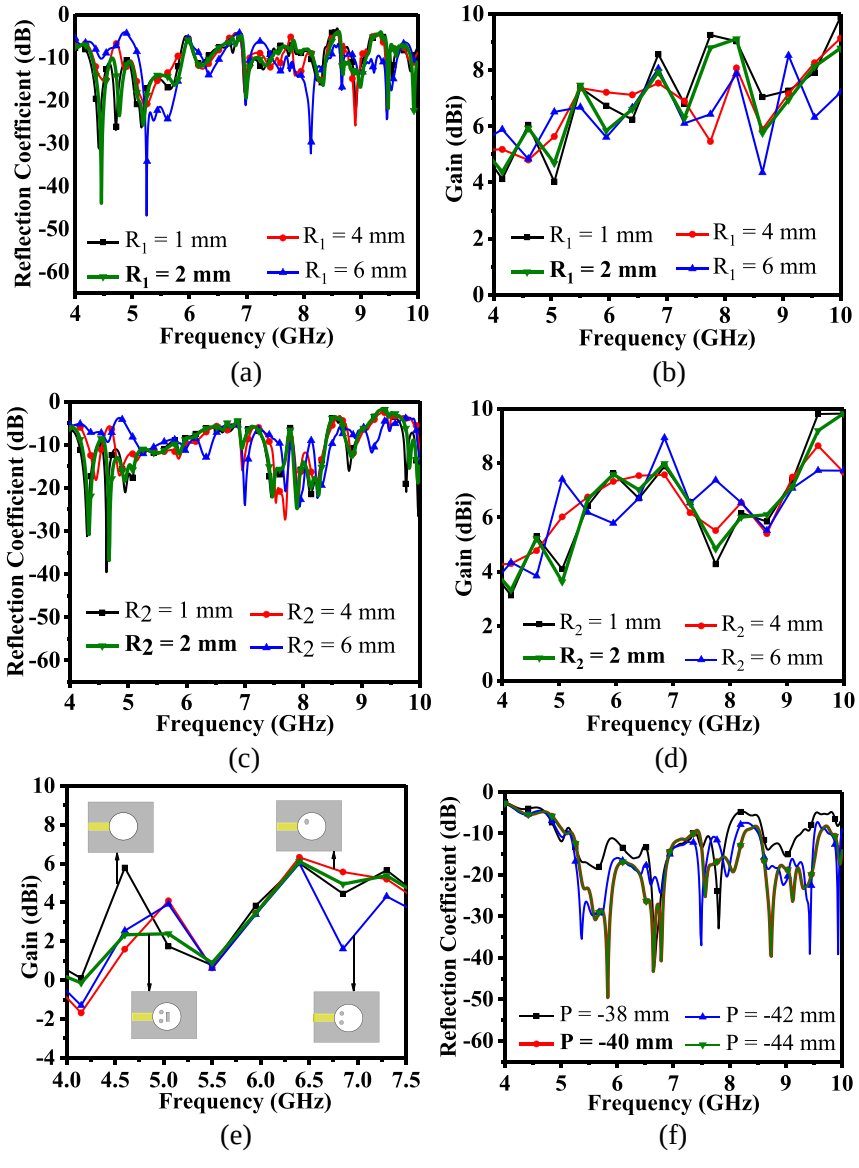

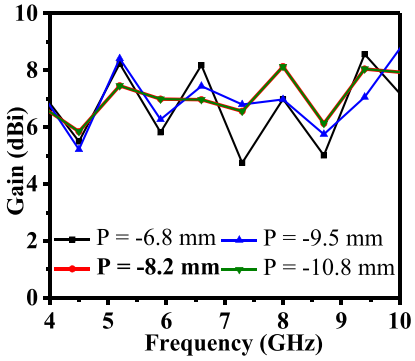

(g)

Figure 4. Parametric study on the circular slot. (a) Reflection coefficient variation of the circular slot of radius R_1. (b) Gain variation of the circular slot of radius R_1. (c) Reflection coefficient variation of the circular slot of radius R_2. (d) Gain variation of the circular slot of radius R_2. (e) Effect of two circular and one rectangular slot on the gain. (f) Effect of two triangular slots on the reflection coefficient. (g) Effect of two triangular slots on the gain.

the impedance bandwidth to 35% at the lower side of the frequency as compared to the other compared radius as shown in Figure 4(c), but at the lower frequency, less than 4 dBi gain is achieved as shown in Figure 4(d). The left frequency shift is observed for $R_1 = 2$ mm and $R_2 = 2$ mm because the higher radiating part of the CDRA is perforated which can be explained by perturbation in the areas of the strong electric field. The effect of this perturbation on the basic CDRA resonant frequency can be understood by the following equations [21].

$$\frac{\omega - \omega_0}{\omega_0} \approx \frac{\iiint\limits_{\Delta\tau} \left(\mu |H_0|^2 - \varepsilon |E_0|^2\right) d\tau}{\iiint\limits_{\tau} \left(\mu |H_0|^2 + \varepsilon |E_0|^2\right) d\tau} \tag{5}$$

The denominator is proportional to the total energy stored, whereas terms in the numerator are proportional to the electric and magnetic energies removed by the perturbation.

$$\frac{\omega - \omega_0}{\omega_0} \approx \frac{\Delta\bar{W}_m - \Delta\bar{W}_e}{W} \tag{6}$$

where W is the total energy stored in the original cavity, and $\Delta\bar{W}_m$ and $\Delta\bar{W}_e$ are time-average electric and magnetic energies originally contained in $\Delta\tau$.

$$\frac{\omega - \omega_0}{\omega_0} \approx \frac{(\bar{w}_m - \bar{w}_e)\,\Delta\tau}{\hat{w}\tau} = C\frac{\Delta\tau}{\tau} \tag{7}$$

The above equation shows that resonant frequency will increase if the perturbation is done at a point of large H (high $\bar{w}_m$), and resonant frequency will decrease if the perturbation is done at a point of large E (high $\bar{w}_e$). However, the combined effect of two circular slots along with one rectangular slot is that the gain of the basic CDRA is increased at the lower frequency of operation as shown in Figure 4(e). The bandwidth obtained for Ant. 2 is slightly higher than Ant. 1, and the peak gain obtained for Ant. 2 is 6.25 dBi at 8.2 GHz, greater than the peak gain of Ant. 1 which is 6.01 dBi at 6.4 GHz.

To design Ant. 3, two triangular slots are removed from the CDRA to further enhance the gain and bandwidth of the antenna. For Ant. 3 effective permittivity is 8.42 which is reduced by 8.47%, resulting in the increase of resonant frequency as shown in Figure 3(a). For enhancing the impedance bandwidth of the antenna, Q factor is an important parameter. By creating two triangle perturbations on the CDRA, the surface area to volume ratio of the antenna is increased, thus reducing the quality factor

and further, improving the impedance bandwidth of the antenna. The bandwidth achieved for Ant. 3 is 38.5% which is greater than the bandwidth of Ant. 2 as shown in Figure 3(a). Further, on Ant. 3, an arc-shaped perturbation is introduced in order to increase the effective path length for the fields. This perturbation also helps increase the effective aperture area, thus improving the gain leading to the final design Ant. 4. For Ant. 3 peak gain obtained is around 8.1 dBi at 8 GHz frequency which is greater than the peak gain obtained for Ant. 2, i.e., 6.2 dBi at 8.2 GHz frequency but less than Ant. 4 peak gain of 8.9 dBi obtained at 9.4 GHz frequency which is clearly depicted in Figure 3(b). The parametric study carried out on Ant. 3 yields that at $P = -40$ mm a wide impedance bandwidth of 50% is obtained which is greater than the other compared positions as shown in Figure 4(f). Point P, as referred from Figure 1(a), refers to the shift of the triangular slots along X-axis where the origin of the coordinate is taken from the center of the structure. The shift in P changes all the triangular slot portions taken together. Figure 4(g) shows the effect of point P on the gain of the CDRA. The maximum gain of 8.9 dBi is obtained at 9.4 GHz. 69.4% impedance bandwidth is obtained by the insertion of one arc shape ceramic at the end of CDRA. At a higher frequency, the gain of the antenna is also improved by the two triangular slots on the CDRA along with the insertion of one arc shape ceramic. The aperture area and radiation boundary of the antenna are increased by the shape of the proposed antenna, thus leading to gain enhancement for the proposed antenna.

2.2. Parametric Study on the Feed Line and Height of the CDRA

By adjusting the width of the microstrip line, the amount of coupling between the microstrip feed line and DRA can be controlled. For the proper selection of the feed length, a parametric study was conducted because the feed length affects the bandwidth of the antenna. Figure 5(a) shows the Feed line length (L) of the proposed antenna. At $L = 40$ mm, 41 mm, 43 mm the antenna's bandwidth performance deteriorates. At $L = 42$ mm wide bandwidth of 69.4% is obtained as shown in Figure 5(b). Table 1 shows the bandwidth obtained at different feed lengths (L).

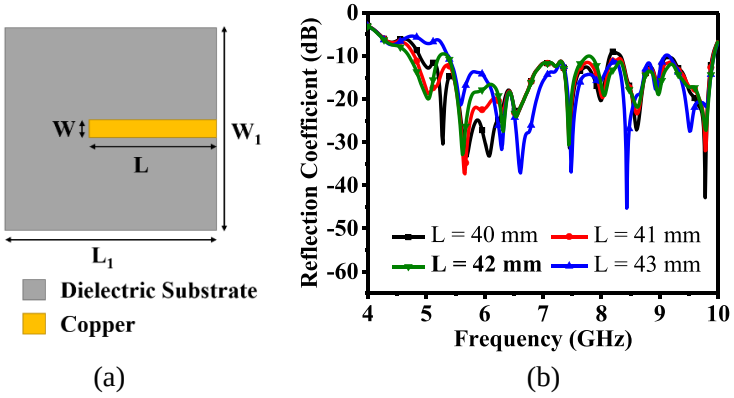

Figure 5. Feed line (L) of the proposed antenna. (a) Geometry. (b) Reflection coefficient.

Table 1. Parametric study on the feed line of the proposed CDRA.

Length of Feedline L (mm)	Bandwidth (GHz)
40	2.8
41	3.2
42	5.0
43	2.9

A parametric study on the height of the CDRA is also done. Figure 6(a) shows the effect of the height of the CDRA on the reflection coefficient, and a complete band of 69.4% is obtained for height

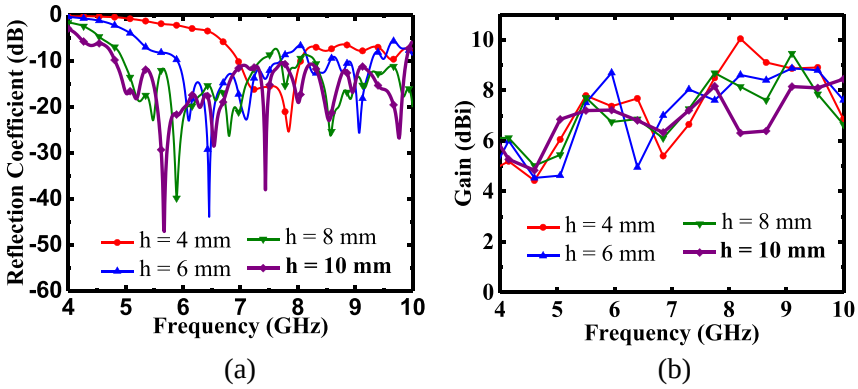

Figure 6. Variation on height h of the proposed structure. (a) Effect of height h of the proposed structure on the reflection coefficient and (b) effect of height h of the proposed structure on the gain.

$h = 10$ mm. Figure 6(b) shows the effect of height on the gain of the CDRA. By observing the graph, it can be found that at $h = 4$ mm maximum peak gain is achieved, but the reflection coefficient is poor; therefore, $h = 10$ mm is chosen in which both gain and reflection coefficient offer the best result.

2.3. Effect of Air Perturbation on the CDRA

Dielectric perturbation is used in mode filtering and mode controlling techniques. Air perturbation, i.e., $\varepsilon_c = 1$ is chosen for the proposed design where ε_c is the permittivity of the cavity, and ε_r is the permittivity of CDRA which is equal to 9.2. By increasing the value of permittivity, a left shift in the resonant frequency is observed because the resonant frequency is reduced by the increase of the permittivity which can be clearly understood by Eqs. (3) and (4) [21].

When $\varepsilon_r < \varepsilon_c$, i.e., for ε_c equal to 20 and 30, and $\varepsilon_r = \varepsilon_c$, i.e., for ε_c equal to 9.2, the first resonance occurs earlier than $\varepsilon_r > \varepsilon_c$, i.e., for ε_c equal to 1 as shown in Figure 7 but increasing the antenna's permittivity, however, significantly reduces the antenna's bandwidth. The absolute permittivity of a dielectric in electromagnetism serves as a gauge for its electric polarizability. When an electric field is applied, a material with a high permittivity polarises more than a material with low permittivity, allowing the material to store more energy; therefore, the quality factor of an antenna is increased by increasing permittivity which results in a decrease in the bandwidth of the antenna. Therefore, bandwidth of the antenna is minimum for $\varepsilon_r < \varepsilon_c$ and $\varepsilon_r = \varepsilon_c$ as compared to $\varepsilon_r > \varepsilon_c$. Thus, air perturbation is chosen for the proposed design.

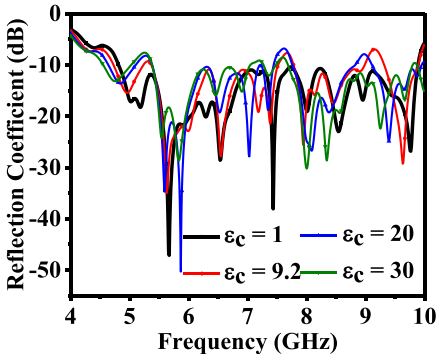

Figure 7. Reflection coefficient versus frequency graph of different dielectric constant of the proposed CDRA.

2.4. Effect of Perturbation on the Effective Permittivity of the CDRA

The quality factor, or Q factor, rises in proportion to the value of permittivity as shown in Eq. (8) [3]. Air cavities in the form of slots are introduced inside the resonator in the proposed design to lower the total effective permittivity of the DR. As a result, resonance will rapidly cause additional electrical and magnetic energy to decay. DR tends to radiate rather than retaining it. Consequently, the impedance bandwidth is increased due to the reduced Q factor. The effective permittivity (ε_{eff}) is calculated by the static capacitance model which is given in Eq. (9) as [11].

$$Q = 2w_0 \frac{\text{Stored Energy}}{\text{Radiated Power}} \propto 2w_0 \left(\varepsilon_{eff}\right)^p \left(\frac{\text{Volume}}{\text{Surface}}\right)^s \text{ with } P > S \geq 1 \tag{8}$$

$$\varepsilon_{eff} = \frac{\varepsilon_r \times V_1 + \varepsilon_C \times V_2}{V_1 + V_2} \tag{9}$$

where ε_r is the permittivity of CDRA which is equal to 9.2, ε_C the permittivity of the cavity which is equal to 1, V_1 the volume of the dielectric layer, and V_2 the volume of the perturbed dielectric layer. For the proposed design effective permittivity is calculated to be 7.97 which is calculated by Eq. (9) and shows that due to the perturbation permittivity is reduced by 13.36% as shown in Table 2.

Table 2. Calculation of effective permittivity for all the four antenna.

Antenna	Formula Used	Values Used (mm)	Effective Permittivity Obtained ε_{eff}	Reduction in permittivity due to Perturbation (%)
Ant. 1	Volume of Ant. 1 cylinder $= \pi \times R^2 \times H$	$R = 20$, $H = 10$	9.2	0
Ant. 2	Volume of two cylindrical slot $C = 2 \times \pi \times R_1^2 \times h$ Volume of one rectangular slot $R = L_2 \times W_2 \times H$ Volume of perturbed dielectric $V_2 = C + R$ Volume of dielectric layer V_1 = Volume of Ant. 1 cylinder − Volume of perturbed dielectric	$R_1 = R_2 = 2$, $H = 10$, $L_2 = 2$, $W_2 = 5.5$	8.96	2.6
Ant. 3	Volume of two triangular slot $T = 2\times \sqrt{S(S-a)(S-b)(S-c)} \times H_1$ Where $S = \frac{a+b+c}{2}$ Volume of perturbed dielectric $V_2 = C + R + T$ Volume of dielectric layer V_1 = Volume of Ant. 1 cylinder − Volume of perturbed dielectric	$a = 14.14$, $b = 17.32$, $c = 11.64$, $H_1 = 5.07$	8.42	8.47
Ant. 4	Volume of arc $A = \frac{\pi \times b \times d}{4} \times H_1$ Volume of perturbed dielectric $V_2 = C + R + T + A$ Volume of dielectric layer V_1 = Volume of Ant. 1 Cylinder − Volume of perturbed dielectric	$b = 17.32$ $d = 10$ $H_1 = 5.07$	**7.97**	**13.36**

2.5. Field Distribution and Analysis

Simulated scalar and vector H-field distributions of the proposed antenna at different frequencies are shown in Figure 8, Figure 9, and Figure 10. From the distributions of the electric field and magnetic field, one can estimate that both the field components are non-zero along the direction of propagation, and therefore it is a hybrid mode for all frequencies. Mode analysis of the proposed CDRA at different frequencies is shown in Figure 11. At frequency 5.6 GHz, $\text{HEM}_{12\delta}$ mode is excited. The electric field

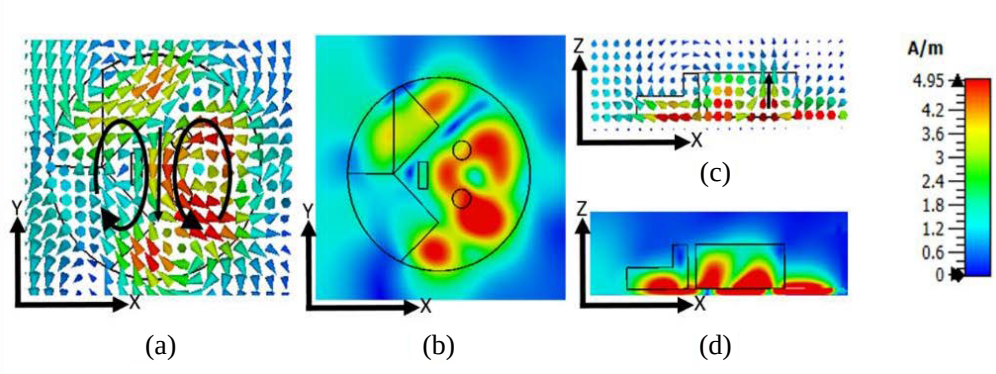

Figure 8. H-field pattern of the prototype at 5.6 GHz: (a) Vector H-field top view, (b) scalar H-field top view, (c) vector H-field side view and (d) scalar H-field side view.

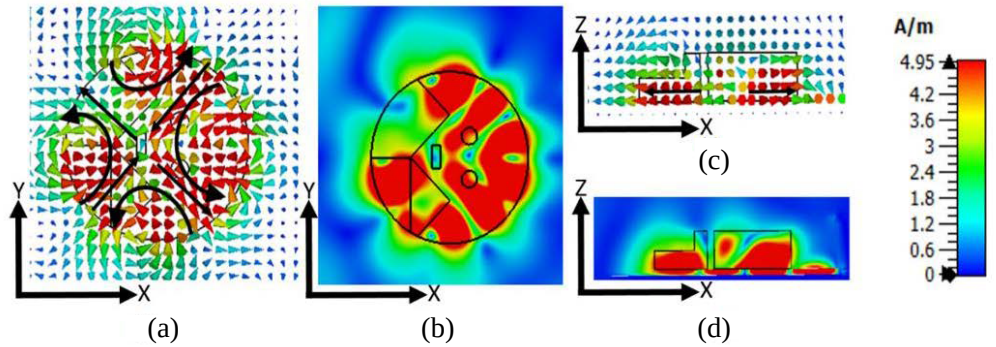

Figure 9. H-field pattern of the prototype at 7.4 GHz: (a) Vector H-field top view, (b) scalar H-field top view, (c) vector H-field side view and (d) scalar H-field side view.

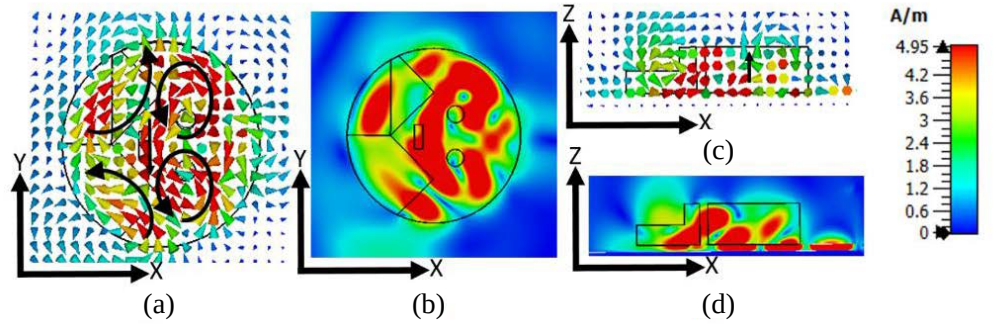

Figure 10. H-field pattern of the prototype at 8.6 GHz: (a) Vector H-field top view, (b) scalar H-field top view, (c) vector H-field side view and (d) scalar H-field side view.

due to the $HEM_{12\delta}$ is linearly polarized. The introduction of two circular air cavities, one rectangular and two triangular cavities removes the electric wall over a selected position on the DRA and simulates unconventional boundary conditions, favoring the excitation of $HEM_{12\delta}$ mode. At frequency 7.4 GHz, $HEM_{21\delta}$ mode is observed. At frequency 8.6 GHz, $HEM_{13\delta}$ mode is observed.

3. RESULTS AND DISCUSSION

Figure 12 shows the fabricated proposed cylindrical dielectric resonator antenna. A high power water jet machine is used for achieving the desired shape on Rogers TMM 10 having a permittivity of 9.2

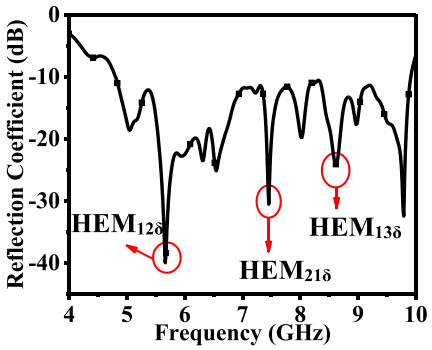

Figure 11. Modes analysis of the proposed CDRA.

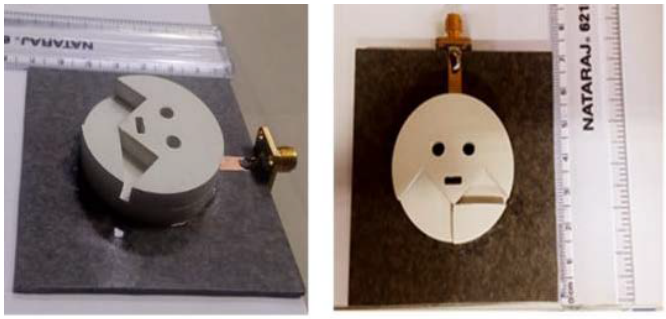

Figure 12. Fabricated proposed cylindrical dielectric resonator antenna. (a) 3-D view, (b) top view.

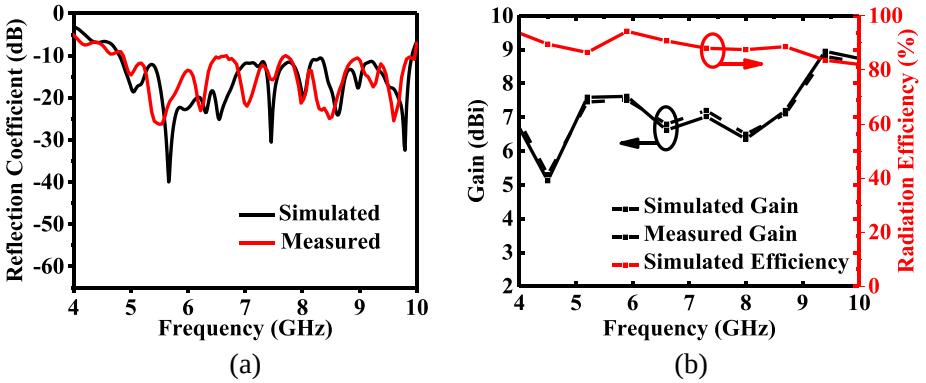

Figure 13. Simulated and measured (a) reflection coefficient, (b) gain and simulated radiation efficiency.

and thickness of 10 mm. After that DRA height of 10 mm and Rogers RT 5880 slab of thickness 1.57 mm having a permittivity of 2.2 are stacked together. For the excitation of the dielectric resonator antenna microstrip feed line is etched on the top side of the Rogers RT 5880 substrate. A commercially available SMA connector is soldered with the feed line and ground plane for the excitation of the fabricated antenna. Agilent E5071C Vector network analyzer is used for the measurement of the reflection coefficient of the fabricated antenna.

The simulated impedance bandwidth of the DRA is 5 GHz (4.8 to 9.8 GHz), and the measured impedance bandwidth of the DRA is 5.04 GHz (4.87 to 9.91 GHz) which clearly illustrate that the measured result is in agreement with the simulated one as shown in Figure 13(a). The minor difference

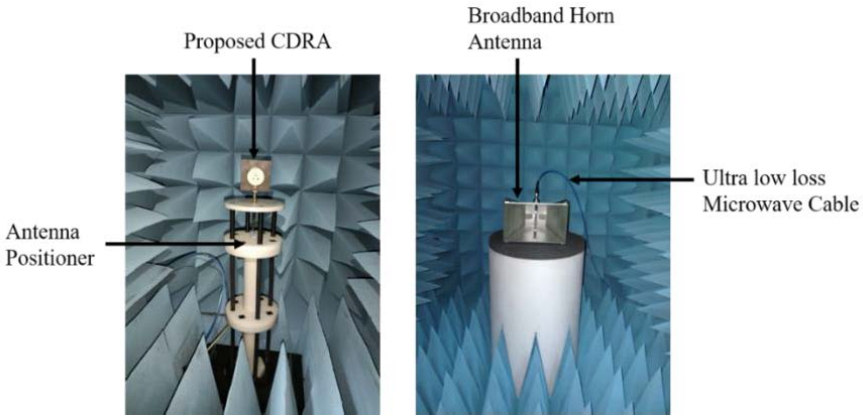

Figure 14. Antenna radiation pattern measurement setup for far field radiation pattern at far field distance.

Table 3. Comparison table of the proposed work with the other simulated work.

Ref.	H	ε_r	R.F (GHz)	B.W (%)	Peak Gain (dBi)	Ant + feed. Tech.
[16]	0.1	10	2.44	4.5	2.54	CRDRA + Coaxial Feed
[17]	0.2	9.8	4.53	51.2	5	Modified DRA + Probe
[18]	0.29	9.8	6	26.95	5.4	CDRA + Aperture Coupled
[19]	0.09	37.4	5.31	3.4	1.97	DRA + Loop Shaped Probe
[20]	0.095	10.2	5.62	47.5	6.84	DRA + Slot + Microstrip Feed
P.S.	**0.16**	**9.2**	**5.6, 7.4, 9.7**	**69.4**	**8.9**	**Cylindrical + Microstrip Feed**

B.W = Bandwidth, CRDRA = Cylindrical Ring Dielectric Resonator Antenna, H = Height of DRA in term of λ_0, P.S. = Proposed Structure, R.F = Resonant Frequency.

in the measured results is attributed to the fabrication tolerances and the effect of stacking the DRAs. Anechoic boxes using two antenna method is used for the measurement of the far field parameters of the proposed antenna. In two antenna method, Dual Ridge Horn DRH20 is used as a transmitter and the proposed antenna used as a receiver. The measured peak gain of 8.9 dBi is achieved at frequency 9.4 GHz, and maximum efficiency of 95% at 5.6 GHz is observed for the proposed antenna as shown in Figure 13(b). The antenna radiation pattern measurement setup for far field radiation pattern is shown in Figure 14. From the radiation pattern plot, it can be observed that at the start of the frequency that is $f = 5.6$ GHz the antenna pattern is directional with very low cross-polarization which is below -15 dB for phi $= 0°$ and -15 dB for phi $= 90°$. For $f = 7.4$ GHz, cross-polarization is below -10 dB for phi $= 0°$ and -15 dB for phi $= 90°$. For $f = 8.6$ GHz, cross-polarization is below -15 dB for phi $= 0°$, and for phi $= 90°$ cross-polarization is below -20 dB. The simulated and measured radiation patterns are shown in Figure 15 for both $\phi = 0°$ and $\phi = 90°$ for the three frequencies as mentioned. The results of the proposed structure and the previously reported work are compared in Table 3. From Table 3, we can observe that the proposed design is better in terms of gain and bandwidth than other compared results. By the use of simple technique (i.e., perturbation), this antenna gives a very wide bandwidth along with high gain. In [16], the $TE_{01\delta}$ mode of a cylindrical ring dielectric resonator antenna has been excited. Impedance bandwidth ranging 2.39–2.50 GHz and the measured gain ranging 2.12–2.54 dBi have been achieved which is less than the proposed work. In [17], a simple cylindrical dielectric resonator undergoes periodic angular deformation along the azimuthal direction. Impedance bandwidth for this antenna ranges from 3.37 to 5.69 GHz which is less than the proposed antenna. In [18], the design of

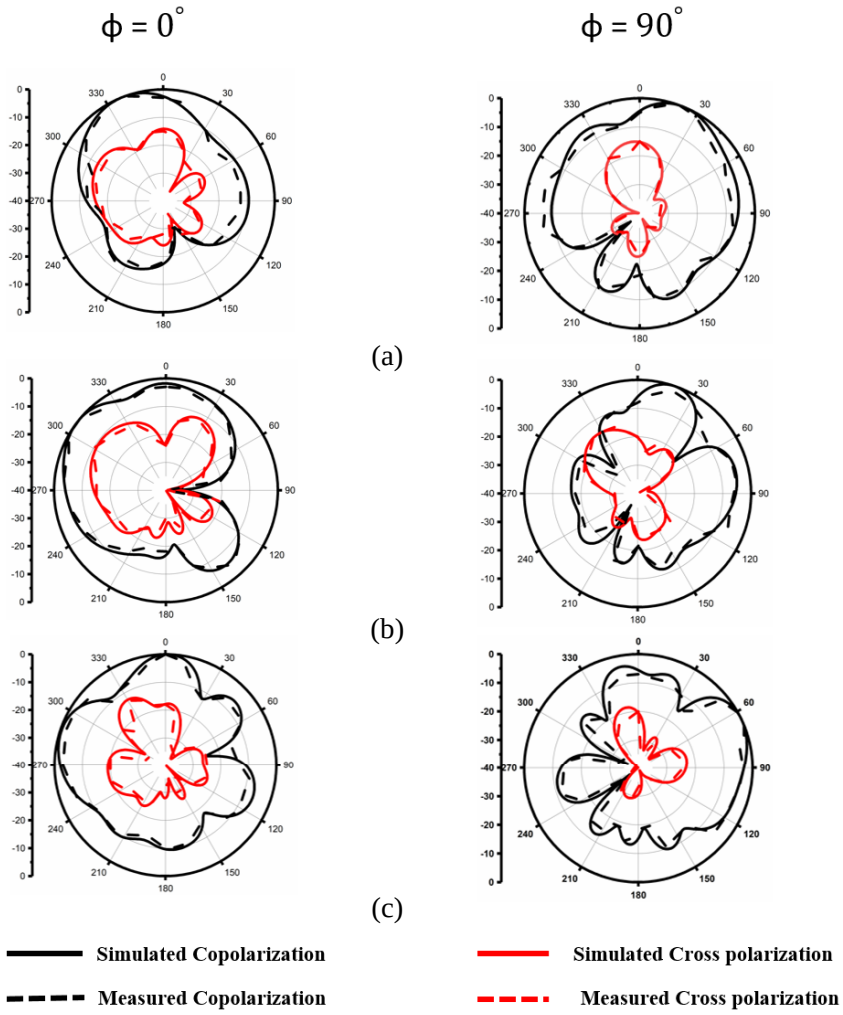

Figure 15. The radiation pattern for the proposed structure for $\phi = 0°$ & $\phi = 90°$. (a) 5.6 GHz, (b) 7.4 GHz and (c) 8.6 GHz.

a unique multi-layered cylindrical ceramic disc antenna with an aperture coupled cylindrical dielectric resonator antenna is proposed. Its frequency band of operation spans from 5.49 GHz to 7.2 GHz, and gain ranges from 5.2 to 5.4 dBi. In [19], for dielectric resonator antennas, a loop-based excitation strategy is described. 1.97 peak gain is achieved which is less than the proposed work. In [20], investigation is conducted into a low-profile DRA that uses air and dielectric vias. Since the proposed antenna gives a very wide bandwidth, it can be used in C-band and ISM band. The proposed structure is found to be novel because to the best of our knowledge such a geometry has not been explored so far. Table 3 indicates that the proposed structure offers better results than the previously reported work.

4. CONCLUSION

In this paper, a low profile CDRA for high gain and wide bandwidth is proposed and investigated. The proposed CDRA is fabricated, measured, and verified with the simulated results. The antenna covers the frequency band from 4.87 GHz to 9.91 GHz and offers a peak gain of 8.9 dBi at 9.4 GHz. The effect of the perturbation on the effective permittivity is calculated, and it is found that ε_{eff} is equal to 7.97 which is reduced by 13.36%. $HEM_{12\delta}$, $HEM_{21\delta}$, and $HEM_{13\delta}$ modes have been identified at 5.6 GHz, 7.4 GHz, and 8.6 GHz, respectively. The proposed antenna finds application in ISM Band and C Band. The proposed structure gives better results despite low profile than the previously reported works.

ACKNOWLEDGMENT

The research described in this paper is supported by the SERB, DST project No.-CRG/2020/000635.

REFERENCES

1. Kiourti, A. and K. S. Nikita, "A review of implantable patch antennas for biomedical telemetry: Challenges and solutions," *IEEE Antennas Propag. Mag.*, Vol. 54, No. 3, 210–228, Jun. 2012.
2. Kiourti, A. and K. S. Nikita, "A review of in-body biotelemetry devices: Implantables, ingestibles, and injectables," *IEEE Trans. Biomed. Eng.*, Vol. 64, No. 7, 1422–1430, Feb. 2017.
3. Petosa, A., *Dielectric Resonator Antenna Handbook*, Artech House, Norwood, MA, USA, Dec. 2007.
4. Pan, Y. M. and S. Y. Zheng, "A low-profile stacked dielectric resonator antenna with high-gain and wide bandwidth," *IEEE Antennas Wirel. Propag. Lett.*, Vol. 15, 68–71, 2016.
5. Dong, X. Y., W. W. Yang, H. Tang, and J. X. Chen, "Wideband low-profile dielectric resonator antenna with a lattice structure," *Electron. Lett.*, Vol. 53, No. 19, 1289–1290, Sep. 2017.
6. Denidni, T. A., Y. Coulibaly, and H. Boutayeb, "Hybrid dielectric resonator antenna with circular mushroom-like structure for gain improvement," *IEEE Trans. Antennas Propag.*, Vol. 57, No. 4, Part 2, 1043–1049, Apr. 2009.
7. Chauhan, M., A. Rajput, and B. Mukherjee, "Wideband circularly polarized low profile dielectric resonator antenna with meta superstrate for high gain," *AEU — Int. J. Electron. Commun.*, Vol. 128, 153524, Dec. 2021.
8. Fakhte, S., H. Oraizi, and L. Matekovits, "Gain improvement of rectangular dielectric resonator antenna by engraving grooves on its side walls," *IEEE Antennas Wirel. Propag. Lett.*, Vol. 16, 2167–2170, May 2017.
9. Chatterjee, A. and S. K. Parui, "Frequency-dependent directive radiation of monopole-dielectric resonator antenna using a conformal frequency selective surface," *IEEE Trans. Antennas Propag.*, Vol. 65, No. 5, 2233–2239, May 2017.
10. Petosa, A. and S. Thirakoune, "Rectangular dielectric resonator antennas with enhanced gain," *IEEE Trans. Antennas Propag.*, Vol. 59, No. 4, 1385–1389, Apr. 2011.
11. Chauhan, M., A. K. Pandey, and B. Mukherjee, "A novel compact cylindrical dielectric resonator antenna for wireless sensor network application," *IEEE Sensors Lett.*, Vol. 2, No. 2, 1–4, Jun. 2018.
12. Gajera, H., D. Guha, and C. Kumar, "New technique of dielectric perturbation in dielectric resonator antenna to control the higher mode leading to reduced cross-polar radiations," *IEEE Antennas Wirel. Propag. Lett.*, Vol. 16, 445–448, 2017.
13. Huang, W. and A. A. Kishk, "Compact wideband multi-layer cylindrical dielectric resonator antennas," *IET Microwaves, Antennas Propag.*, Vol. 1, No. 5, 998–1005, Nov. 2007.
14. Chair, R., A. A. Kishk, and K. F. Lee, "Wideband simple cylindrical dielectric resonator antennas," *IEEE Microw. Wirel. Components Lett.*, Vol. 15, No. 4, 241–243, Apr. 2005.
15. Kajfez, D., A. W. Glisson, and J. James, "Computed modal field distributions for isolated dielectric resonators," *IEEE Trans. Microw. Theory Tech.*, Vol. 32, No. 12, 1609–1616, Dec. 1984.
16. Liu, T., H. Yang, Y. He, and J. Lu, "A TE mode omnidirectional dielectric resonator antenna excited by a special configuration," *IEEE Trans. Antennas Propag.*, Vol. 66, No. 12, 7339–7341, Dec. 2018.
17. Chowdhury, R. and R. K. Chaudhary, "An approach to generate circular polarization in a modified cylindrical-shaped dielectric resonator antenna using PMC boundary approximation," *IEEE Antennas Wirel. Propag. Lett.*, Vol. 17, No. 9, 1727–1731, Sep. 2018.
18. Mashhadi, S. H. H., Y. C. Jiao, and J. Chen, "Broadbeam cylindrical dielectric resonator antenna," *IEEE Access*, Vol. 7, 112653–112661, Aug. 2019.
19. Seko, M. H. and F. S. Correra, "Excitation of dielectric resonator antennas by loop coupling," *IEEE Antennas Wirel. Propag. Lett.*, Vol. 18, No. 4, 656–658, Apr. 2019.

20. Kremer, H. I., K. W. Leung, and M. W. K. Lee, "Compact wideband low-profile single-and dual-polarized dielectric resonator antennas using dielectric and air vias," *IEEE Trans. Antennas Propag.*, Vol. 69, No. 12, 8182–8193, Jun. 2021.
21. Harrington, R. F., *Time-harmonic Electromagnetic Field*, McGraw-Hill, New York, 1961.